

Targeting high symmetry in structure predictions by biasing the potential energy surface

Hannes Huber,¹ Martin Sommer,¹ Moritz Gubler,¹ and Stefan Goedecker¹

¹*Department of Physics, University of Basel, Klingelbergstrasse 82, CH-4056 Basel, Switzerland*

Ground state structures found in nature are in many cases of high symmetry. But structure prediction methods typically render only a small fraction of high symmetry structures. Especially for large crystalline unit cells there are many low energy defect structures. For this reason methods have been developed where either preferentially high symmetry structures are used as input or where the whole structural search is done within a certain symmetry group. In both cases it is necessary to specify the correct symmetry group beforehand. However it can in general not be predicted which symmetry group is the correct one leading to the ground state. For this reason we introduce a potential energy biasing scheme that favors symmetry and where it is not necessary to specify any symmetry group beforehand. On this biased potential energy surface, high symmetry structures will be found much faster than on an unbiased surface and independently of the symmetry group to which they belong. For our two test cases, a C_{60} fullerene and bulk silicon carbide, we get a speedups of 25 and 63. In our data we also find a clear correlation between the similarity of the atomic environments and the energy. In low energy structures all the atoms of a species tend to have similar environments.

Structure prediction methods are an important tool for the discovery of new materials [1]. Such methods can not only be applied for materials at ambient pressure but also under very high pressures that are relevant for geophysical applications, but not accessible by experimental methods [2]. For this reason, numerous methods such as simulated annealing [3], basin hopping [4], minima hopping (MH) [5–8], random structure searches [9], meta-dynamics [10] and various variants of evolutionary genetic algorithms [11–16] as implemented in the USPEX [17], CALYPSO [18] and XtalOpt [19] software package have been developed. These advanced global geometry optimisation methods have shown that they can efficiently explore [20, 21] the potential energy surface (PES) of different clusters and bulk materials under a variety of external conditions and predict new structures. However, such methods require a high computational effort because the number of possible meta-stable structures grows exponentially with respect to the number of atoms in the system and the generation and relaxation of a single structure requires many energy and force evaluations.

Unless defects of certain materials are studied explicitly, the ground state and the lowest defect free meta-stable structures are of greatest interest since they are the structures that can most likely be synthesized. However, for large cells most structures that are found in a structure prediction contain defects. Typically these defect structures represent local minima in a funnel whose bottom corresponds to a defect-free, meta-stable or the global minimum structure. To find this relatively small number of defect-free structures, a structure search which visits a very large number of defect structures, is inefficient.

To favor high symmetry, most crystal structure prediction methods use input guess structures that are of high symmetry. If the correct symmetry is chosen, the most similar low energy structure is found much more rapidly. For basin hopping and genetic algorithms there exist also a versions where all the moves of the atoms are constrained to conserve the desired symmetry [4, 22]. The inconvenience in all these approaches is that there are more than 200 space groups and it is a priori unknown which one will be adopted by the system. Traditionally symmetry is defined by geometric operations such as rotations or reflections that leave the structure invariant. We will use

in this work an alternative definition of symmetry. We will consider a system to be highly symmetric if all atoms of the same element see only a small number of different environments. Structures with a large number of environments are actually unlikely to exist according Pauling’s rule of structural parsimony originally established for ionic materials [23, 24]. In many cases we will actually try to find systems where all atoms of the same element see the same environment. Evidently this is true for many high symmetry structures such as the C_{60} fullerene or the diamond structure of silicon and carbon. A structure is either invariant or not under certain symmetry operations. So basing some penalty function on the number of possible symmetry operations would give rise to a discontinuous function. Our definition of similarity is however a continuous functions. It is zero if the environments are identical and grows larger in a continuous way when the environments become more different. Our definition is thus broader than the traditional one. We classify a structure also as highly symmetric if there are a few distinct environments which are however very similar.

The tendency that low energy structures have in general similar environments has already been exploited to gain efficiency in the context of evolutionary structure prediction algorithms. In this context mutation moves were introduced that favor environments that have a similar radial distribution as certain selected role model environments [25, 26]. Even in amorphous systems it was observed that structures that had similar pair distribution functions were also low in energy [27].

The basic idea of our approach is to perform a structure search on a biased potential energy surface [28]

$$E_b(R_1, \dots, R_n) = E(R_1, \dots, R_n) + \omega P(R_1, \dots, R_n)$$

where E_b is the biased PES, E is the physical PES, P is the penalty function and ω is the biasing weight. Since the number of environments is larger for defective structures, the penalty part will push up these defective structures on the biased PES. In this way the downhill barriers are lowered compared to the uphill barriers and the PES becomes a stronger structure seeker character which speeds up the search for the global minimum and possibly other high symmetry structures at the bottom of other funnels.

We quantify the similarity of environments with the overlap matrix (OM) fingerprint [29] based on s- and p-type orbitals, that was shown to be able to detect in a highly reliable way different atomic environments [30]. In particular this fingerprint has both radial and angular resolution. In the OM method the eigenvalues of a localized overlap matrix, centered on the atom i whose environment has to be characterized, are assembled into an atomic environment fingerprint vector \mathbf{f}_i . This environment characterization is done for all atoms in the system. If all atomic environments are identical, the rank of the matrix F formed by all these vectors \mathbf{f}_i is one, if there are two distinct elemental environments the rank is two, etc. The rank can most easily be calculated from the eigenvalues λ_i of the Gram matrix $D = F^T F$, constructed from these fingerprint vectors. The number of the non-zero eigenvalues of this matrix gives the rank of the fingerprint vectors. So the penalty function that favours one single environment for a certain element is

$$P_1(R_1, \dots, R_{N_{at}}) = \sum_{i=2}^{N_{at}} \lambda_i = \text{Tr}(D) - \lambda_1, \quad (1)$$

In case we want to allow for up to two environments, the penalty becomes

$$P_2(R_1, \dots, R_{N_{at}}) = \sum_{i=3}^{N_{at}} \lambda_i = \text{Tr}(D) - \lambda_1 - \lambda_2, \quad (2)$$

where Tr is the trace of the matrix, i.e. the sum over all eigenvalues. As usual, we have assumed in all the above formulas that the eigenvalues are sorted in decreasing order. For a multi-component system, each element contributes its own penalty function and the total penalty function is the sum of all the elemental contributions. For highly symmetric structures where all local environments are equivalent, e.g. the ground state of C_{60} , the bias function will be exactly zero. If the environments get more distinct, the bias function grows due to the positive semi-definiteness of the Gram matrix. Since the Gram matrix gives essentially the effective dimension of the vector space spanned by the local descriptor vectors, it is called dimensionality matrix in this paper.

To test our method we selected two systems of quite different nature. The first one, silicon carbide, is a crystalline system with two elements that have to mix in the right way to find low energy structures and the second, the C_{60} fullerene, is a molecular clusters. Its global minimum is just one structure out of a huge number of meta-stable structures with varying structural motifs such as planar structures, chains and bowls.

For the exploration of the PES the minima hopping (MH) algorithm was used, but our biasing scheme is in principle applicable to any structure prediction method. The MH algorithm is not based on thermodynamic principles like simulated annealing or basin hopping but uses a combination of molecular dynamics, local geometry optimization and a history of previously found local minima to escape quickly from already known regions and hence, efficiently explore the entire PES. For the geometry optimization of C_{60} with free boundary conditions the conjugate gradient method was used. In the case of periodic boundary conditions (PBC) the highly efficient and stable

vc-SQNM method developed by Gubler et al. [31, 32] was used. The molecular dynamics (MD) simulation was implemented using the velocity Verlet algorithm for the non-periodic case and the variable cell shape MD [33] for PBC. This method allows atoms as well as cell vectors to move dynamically during the MD simulation for PBC.

For the calculation of the PES of C_{60} the transferable tight binding potential for carbon from Xu et al. [34] was used. For the silicon carbide simulations in PBC DFTB+ [35] was used with the Slater-Koster parameterisation set pbc-0-3 [36]. The MD and an initial local geometry optimisation are performed on the biased PES followed by a local geometry optimisation on the unbiased PES. This avoids falling in potentially existing spurious local minima on the biased PES.

To obtain conservative forces of the biased PES the derivative of the symmetry bias needs to be added to the physical forces. The same is true for the derivative of the biased symmetry function with respect to the lattice vectors which need to be added to the lattice derivatives in the case of PBC. The derivations of these two quantities can be found in the supplementary information.

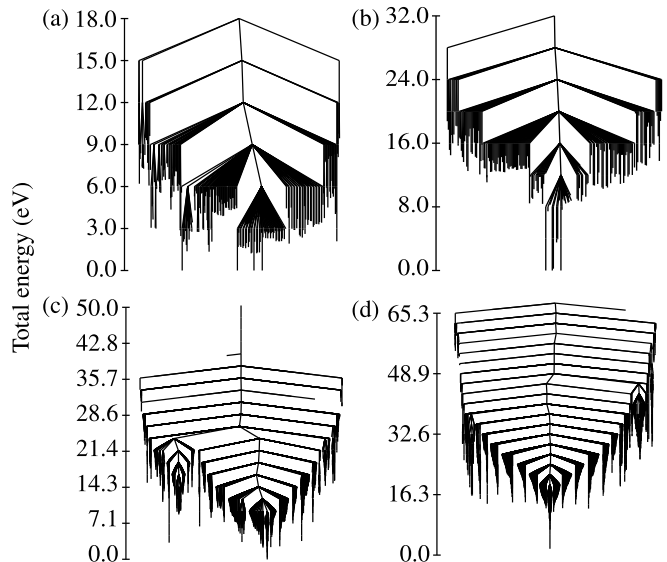


Figure 1. Changes in the characteristics of the disconnectivity graphs of silicon carbide (top row) and C_{60} (bottom row) induced by a bias. The left column shows the disconnectivity graphs of the PES without a bias and the right column the disconnectivity graphs of the PES with a bias. The graph was constructed with the disconnectDPS software [37].

The character of a PES can best be deduced from the appearance of its disconnectivity graph [38] Fig. 1. For a structure seeker [39], the downhill barriers are much lower than the uphill barriers. As a consequence, any algorithm that crosses preferentially lower barriers will experience some driving force toward the minimum at the bottom of the funnel and find it therefore faster. This driving force will of course depend on the strength ω of the bias. While on the one hand it is desirable to choose a large ω , the penalty should on the other hand only induce some weak perturbation that does not completely

deform the physical PES. In particular there should remain in most cases a one-to-one mapping between the local minima on the physical and the biased PES. As already noted by Zwanzig in the context of protein folding [40] a relatively small bias can have a large effect on the dynamics of the system and reduce the folding time by several orders of magnitude. We were indeed always able to find a range of values for ω that did speed up the search for high symmetry structures considerable without destroying the overall character of the PES. With our weight the downhill barriers are typically twice as large as the uphill barriers and the penalty difference between high and low symmetry structures is a few times the difference of their physical energy. This later criterion can be used to find suitable values of ω .

Fig. 1 shows the differences of the disconnectivity graphs for the unbiased and biased system. The changes in the appearance of the disconnectivity graphs indicate that the biased PES has a much stronger structure seeker character which should make the search for the lowest high symmetry structures considerably faster.

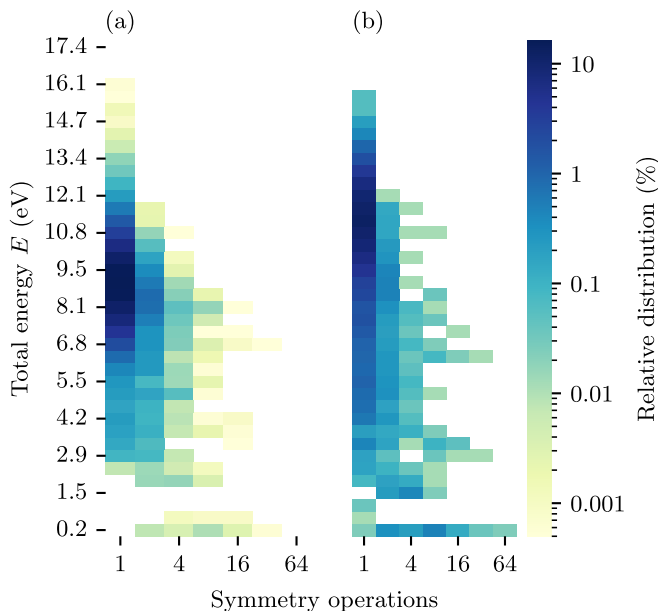


Figure 2. Comparison of the distribution of the found minima on the unbiased (a) and biased (b) PES. The symmetry, plotted along the x-axis, is measured by the number symmetry operations that leave the structure invariant. The coloring indicates the relative abundance of meta-stable structures for a given symmetry and energy.

To investigate the effect of the symmetry bias on the speed of the global geometry optimization in a systematic way, statistical tests were conducted for C_{60} and 16 atom silicon carbide cells. One hundred global geometry optimizations were started from different initial configurations until the ground state structure, or in the case of silicon carbide a polytype of the ground state, was found on the unbiased and the biased PES. For C_{60} the carbon atoms were randomly placed on a plane and for silicon carbide the carbon and silicon atoms were randomly placed in spatially separated sub-cells that formed the crystalline cell. To avoid nonphysical structures a minimum and maximum

distance between the randomly placed atoms was enforced. Since there are no phase separated low energy structures in a cell of this size, the silicon and carbon atoms always had to mix to find the low energy structures. As a measure for the computational cost of the runs we used the number of required local geometry optimizations. As can be seen from Table I the biasing reduces the average number of geometry optimizations by a factor of 25 for C_{60} and by a factor of 63 for silicon carbide. It can also be seen from Table I that other statistical markers like the standard deviation (std), quantiles and the number of geometry optimizations for the fastest as well as the slowest simulations decreased by about the same magnitude. As expected

Table I. Table of statistical markers and biasing parameters of 100 global geometry optimisations started from randomly generated structures for C_{60} and 16 atom silicon carbide cells on the unbiased PES as well as on the biased PES. The statistical markers always relate to the required number of local geometry optimisations. The biasing parameters for C_{60} were $\omega = 0.3$ with $\sigma_c = 6.0$ [29] and for silicon carbide $\omega = 3.5$ with $\sigma_c = 4.5$. The numbers in parenthesis give the speedup with respect to the unbiased runs for corresponding quantities. All simulations were successfully carried out until the ground state structure or in the case of 16 atom silicon carbide a polytype of the ground state structure, was found.

	C_{60} unbiased	C_{60} biased	SiC unbiased	SiC biased
mean	9254.71	370.87 (25)	9715.36	153.84 (63)
std	7716.87	246.74 (31)	10181.81	97.92 (104)
min	1184	89 (13)	771	31 (25)
25%	4048	180 (22)	3506	87 (40)
50%	6994	309 (23)	5720	122 (47)
75%	11765	520 (23)	12170	202 (60)
max	44136	1165 (38)	56213	571 (98)

and as shown in Fig. 2 the distribution of the found structures with respect to their physical energy E and their degree of symmetry is also quite different. For the biased MH runs, the fraction of high symmetry structures is considerably higher and the average physical energy of low symmetry structures is higher since many low energy defects were not found. Many of these high symmetry structures are quite interesting. Searching for structures where all atoms of a certain species have the same environment, we found for instance several SiC structures where all the carbon atoms were 3-fold coordinated, whereas all the silicon atoms are 4-fold coordinated. Such a structure is shown in Fig. 3. Since our penalty function goes smoothly to zero when the environments get more similar, we actually also found most low energy structures of silicon carbide with up to 4 different environments per atom with a penalty function that favours a single environment. It turned out that in these cases, the environments tend to be quite similar and result thus in a small instead of a strictly zero penalty function (see Fig. 3). This finding is related to a strong correlation between the structural environment diversity as measured by our penalty function and the total energy as shown in Fig. 4.

In summary, based on a non-conventional measure of symmetry, that is motivated by Paulings rule of parsimony, we construct a penalty function that measures the dissimilarity between different atomic environments in a structure. To construct the penalty function no guesses of which symmetry will be adopted

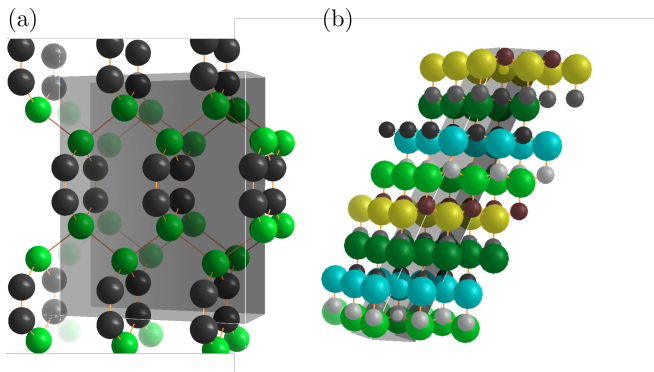


Figure 3. Two high symmetry structures found by a biased run. The structure (a) is only 517 meV/atom higher in energy than the ground state structure, even though the bonding character is completely different from the ground state where all atoms are 4-fold coordinated. In this structure all carbon atoms are 3-fold coordinated. Structure (b) is a 4-fold coordinated silicon carbide structure with an energy of 6 meV/atom above the ground state. Four different environments exist for each carbon and silicon atom, but the environments are so similar that the differences can not be detected by eye. Carbon atoms are displayed by smaller spheres than silicon atoms for which each environment has its own colour.

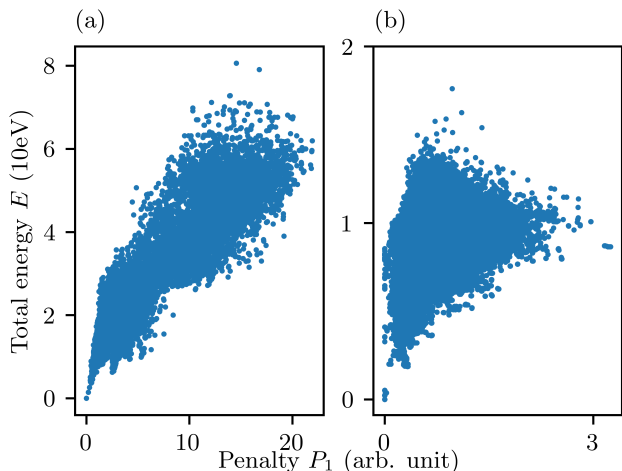


Figure 4. Correlation between our penalty function P_1 , that is a measure of the structural diversity and the total energy E . Only if all atoms in the C_{60} (a) or silicon carbide (b) structure have similar environments, the energy of the structure will be low.

by the system are required. Adding this penalty function to the physical PES gives a biased PES where disordered structures are pushed up in energy relative to high symmetry structures. This leads to a lowering of the downhill barriers compared to the uphill barriers. This stronger structure seeker property of the biased potential energy surface allows for much faster searches for high symmetry ground states.

The penalty function also allows us to find high symmetry structures of higher energy rapidly. This feature opens the way to perform structure prediction on a PES that was constructed with a cheap but not very accurate method to find high sym-

metry structures in low as well as moderately higher energy regions. These high symmetry structures can then be reranked by calculating their energies with a more accurate but also more expensive electronic structure method. In this way high energy structures that were higher in energy with the cheap method can become low in energy with the accurate method. This procedure would not be possible without the bias because in this case the overwhelming majority of higher energy structures are typically all defect structures, which are unlikely to become low energy structures when reranked.

Our results also clearly show the general validity of Paulings rule that in low energy structures the variability of the atomic environments is quite limited.

Financial support from SNF and computing time from CSCS (project s963) and sciCORE (<http://scicore.unibas.ch/>) are acknowledged. We thank Prof. Alireza Ghasemi and Prof. Andris Gulans for useful comments on the manuscript.

- [1] A. R. Oganov, C. J. Pickard, Q. Zhu, and R. J. Needs, *Nature Reviews Materials* **4**, 331 (2019).
- [2] K. P. Hilleke, T. Bi, and E. Zurek, *APPLIED PHYSICS A-MATERIALS SCIENCE & PROCESSING* **128** (2022), [10.1007/s00339-022-05576-z](https://doi.org/10.1007/s00339-022-05576-z).
- [3] S. Kirkpatrick, C. D. Gelatt, and M. P. Vecchi, *Science (New York, N.Y.)* **220**, 671 (1983).
- [4] D. J. Wales and J. P. K. Doye, *The Journal of Physical Chemistry A* **101**, 5111 (1997).
- [5] S. Goedecker, *The Journal of Chemical Physics* **120**, 9911 (2004), <https://doi.org/10.1063/1.1724816>.
- [6] M. Amsler and S. Goedecker, *The Journal of chemical physics* **133**, 224104 (2010).
- [7] M. Sicher, S. Mohr, and S. Goedecker, *The Journal of chemical physics* **134**, 044106 (2011).
- [8] S. Roy, S. Goedecker, and V. Hellmann, *Physical Review E* **77**, 056707 (2008).
- [9] C. J. Pickard and R. J. Needs, *Phys. Rev. Lett.* **97**, 045504 (2006).
- [10] R. Martoňák, A. R. Oganov, and C. W. Glass, *Phase Transitions* **80**, 277 (2007), <https://doi.org/10.1080/01411590701228398>.
- [11] R. L. Johnston, *Dalton Transactions*, 4193 (2003).
- [12] A. R. Oganov and C. W. Glass, *The Journal of chemical physics* **124**, 244704 (2006).
- [13] S. Bhattacharya, S. V. Levchenko, L. M. Ghiringhelli, and M. Scheffler, *Phys. Rev. Lett.* **111**, 135501 (2013).
- [14] L. B. Vilhelmsen and B. Hammer, *The Journal of chemical physics* **141**, 044711 (2014).
- [15] Q. Zhu, A. R. Oganov, A. O. Lyakhov, and X. Yu, *Physical Review B* **92** (2015), <https://doi.org/10.1103/PhysRevB.92.024106>.
- [16] F. Curtis, X. Li, T. Rose, Á. Vázquez-Mayagoitia, S. Bhattacharya, L. M. Ghiringhelli, and N. Marom, *Journal of chemical theory and computation* **14**, 2246 (2018).
- [17] C. W. Glass, A. R. Oganov, and N. Hansen, *Computer Physics Communications* **175**, 713 (2006).
- [18] Y. Wang, J. Lv, L. Zhu, and Y. Ma, *Comput. Phys. Commun.* **183**, 2063 (2012).
- [19] Z. Falls, P. Avery, X. Wang, K. P. Hilleke, and E. Zurek, *The Journal of Physical Chemistry C* **125**, 1601 (2021).
- [20] M. S. Jørgensen, U. F. Larsen, K. W. Jacobsen, and B. Hammer, *The journal of physical chemistry. A* **122**, 1504 (2018).
- [21] T. Yamashita, N. Sato, H. Kino, T. Miyake, K. Tsuda, and T. Oguchi, *Physical Review Materials* **2** (2018), <https://doi.org/10.1103/PhysRevMaterials.2.013803>.
- [22] S. E. Wheeler, P. v. R. Schleyer, and H. F. Schaefer, *The Journal of Chemical Physics* **126**, 104104 (2007), <https://doi.org/10.1063/1.2646940>.
- [23] L. Pauling, *Journal of the American Chemical Society* **51**, 1010 (1929).
- [24] L. Pauling, *The nature of the chemical bond and the structure of molecules and crystals: An introduction to modern structural chemistry*, 3rd ed. (Cornell Univ. Pr, Ithaca, NY, 1989).
- [25] K. H. Sørensen, M. S. Jørgensen, A. Bruix, and B. Hammer, *The Journal of Chemical Physics* **148**, 241734 (2018), <https://doi.org/10.1063/1.5023671>.
- [26] S. Chiriki, M.-P. V. Christiansen, and B. Hammer, *Phys. Rev. B* **100**, 235436 (2019).
- [27] M. J. Cliffe, A. P. Bartók, R. N. Kerber, C. P. Grey, G. Csányi, and A. L. Goodwin, *Phys. Rev. B* **95**, 224108 (2017).
- [28] D. S. De, M. Krummenacher, B. Schaefer, and S. Goedecker, *Physical review letters* **123**, 206102 (2019).
- [29] L. Zhu, M. Amsler, T. Fuhrer, B. Schaefer, S. Faraji, S. Rostami, S. A. Ghasemi, A. Sadeghi, M. Grauzinyte, C. Wolverton, *et al.*, *The Journal of chemical physics* **144**, 034203 (2016).
- [30] B. Parsaeifard, D. Tomerini, D. S. De, and S. Goedecker, *The Journal of chemical physics* **153**, 214104 (2020).
- [31] M. Gubler, M. Krummenacher, H. Huber, and S. Goedecker, “Efficient variable cell shape geometry optimization,” (2022).
- [32] B. Schaefer, S. Alireza Ghasemi, S. Roy, and S. Goedecker, *The Journal of chemical physics* **142**, 034112 (2015).
- [33] M. Parrinello and A. Rahman, *Journal of Applied Physics* **52**, 7182 (1981), <https://doi.org/10.1063/1.328693>.
- [34] C. Xu and G. E. Scuseria, *Physical review letters* **72**, 669 (1994).
- [35] B. Hourahine, B. Aradi, V. Blum, F. Bonafé, A. Buccheri, C. Camacho, C. Cevallos, M. Y. Deshayé, T. Dumitrică, A. Dominguez, S. Ehlert, M. Elstner, T. van der Heide, J. Hermann, S. Irle, J. J. Kranz, C. Köhler, T. Kowalczyk, T. Kubař, I. S. Lee, V. Lutsker, R. J. Maurer, S. K. Min, I. Mitchell, C. Negre, T. A. Niehaus, A. M. N. Niklasson, A. J. Page, A. Pecchia, G. Penazzi, M. P. Persson, J. Řezáč, C. G. Sánchez, M. Sternberg, M. Stöhr, F. Stuckenberg, A. Tkatchenko, V. W.-Z. Yu, and T. Frauenheim, *The Journal of chemical physics* **152**, 124101 (2020).
- [36] A. Sieck, “Structure and physical properties of silicon clusters and of vacancy clusters in bulk silicon,” (2000).
- [37] M. Miller, D. Wales, and V. de Souza, “disconnectionDPS: Fortran program to generate disconnectivity graphs from stationary point databases.” <http://www-wales.ch.cam.ac.uk/software.html> (2022).
- [38] O. M. Becker and M. Karplus, *J. Chem. Phys.* **106**, 1495 (1997).
- [39] D. Wales, *Energy Landscapes: Applications to Clusters, Biomolecules and Glasses*, 1st ed. (Cambridge University Press, 2004).
- [40] R. Zwanzig, A. Szabo, and B. Bagchi, *Proceedings of the National Academy of Sciences* **89**, 20 (1992), <https://www.pnas.org/content/89/1/20.full.pdf>.

Appendix A: Symmetry Bias

The goal of the symmetry bias is to find a measure for the structural symmetry of the system and to use it as a bias on the PES to drive the system faster to the global minimum during a minima hopping simulation. As a measure for the structural symmetry of a system we quantify the differences between the individual atomic environments.

First a matrix F is formed containing the overlap matrix (OM) fingerprints [29] of every atom k of the cluster or cell as vector V_k in columns. In the OM fingerprint method the eigenvalues of a localized overlap matrix are assembled into a vector. All entries of each fingerprint vectors V_k need to be sorted before forming the matrix F .

$$F = \begin{pmatrix} V_1(1) & V_2(1) & V_3(1) & \cdots & V_{N_{at}}(1) \\ V_1(2) & V_2(2) & V_3(2) & \cdots & V_{N_{at}}(2) \\ \vdots & \vdots & \vdots & \ddots & \vdots \\ V_1(l_{fp}) & V_2(l_{fp}) & V_3(l_{fp}) & \cdots & V_{N_{at}}(l_{fp}) \end{pmatrix}$$

with $V_k(j)$ being the j -th entry of the OM fingerprint and l_{fp} is the length of the fingerprint vectors.

The Gram matrix

$$D = F^T F \quad (\text{A1})$$

can now be formed.

If all atomic environments are identical, the rank of the matrix D formed by the OM fingerprint vectors is one, when there are only two different environments the rank is two, etc. The rank can most easily be calculated from the eigenvalues λ_i of the matrix D , constructed from the OM fingerprint vectors. The eigenvalues λ_i of matrix D are sorted in descending order, i.e. λ_1 is the largest eigenvalue. The matrix elements $D_{i,j}$ equals $\langle V_i | V_j \rangle$ for the atom pair (i, j) .

The number of the non-zero eigenvalues of this matrix gives the rank of the fingerprint vectors. So the penalty function that favours one single environment for a certain element is

$$P_1(R_1, \dots, R_{N_{at}}) = \sum_{i=2}^{N_{at}} \lambda_i = \text{Tr}(D) - \lambda_1, \quad (\text{A2})$$

In case we want to allow for up to l environments, the penalty becomes

$$P_l(R_1, \dots, R_{N_{at}}) = \sum_{i=l+1}^{N_{at}} \lambda_i = \text{Tr}(D) - \sum_{i=1}^l \lambda_i \quad (\text{A3})$$

where R_i is the position of the atom i in the system in Cartesian coordinates, N_{at} equals the number of atoms in the system and $\text{Tr}(D)$ is the trace of matrix D .

For a multi-component system, each element contributes its own penalty function and the total penalty function is the sum of all the elemental contributions.

Appendix B: Symmetry bias derivatives

To obtain conservative forces of the biased PES the derivative of the symmetry bias needs to be added to the physical forces. The same is true for the derivative of the biased symmetry function with respect to the lattice vectors which need to be added to the lattice derivatives in the case of PBC.

1. Symmetry bias derivative with respect to atomic coordinates

The derivative of the symmetry bias function with respect to the atomic coordinates is

$$\frac{\partial P}{\partial R} = \frac{\partial(\text{Tr}(D) - \lambda_1)}{\partial R} = \sum_i \left(\frac{\partial D_{i,i}}{\partial R} \right) - \frac{\partial \lambda_1}{\partial R}. \quad (\text{B1})$$

For the term $\frac{\partial \lambda_1}{\partial R}$ the Hellman Feynman Theorem is used.

$$\frac{\partial \lambda_1}{\partial R} = \langle X_1 | \frac{\partial D}{\partial R} | X_1 \rangle$$

with X_1 being the eigenvector belonging to the largest eigenvalue λ_1 of matrix D . The derivative of the dimensionality matrix $\frac{\partial D}{\partial R}$ depends on the derivatives of the OM fingerprints.

$$\frac{\partial D_{i,j}}{\partial R} = \sum_l \frac{\partial V_i(l)}{\partial R} V_j(l) + \frac{\partial V_j(l)}{\partial R} V_i(l) \quad (\text{B2})$$

with l counting over all entries in the atomic fingerprint eigenvectors V_i . The derivative $\frac{\partial V_i}{\partial R}$ is formed with the help of publication [29].

Now the negative gradient of the derivative can be added to the physical forces to obtain the biased forces belonging to the biased PES.

2. Symmetry bias derivative with respect to lattice vectors

Analog to the derivative with respect to the atom positions we can find the derivative with respect to the lattice vectors

$$\frac{\partial P}{\partial \mathbf{h}} = \frac{\partial(\text{Tr}(D) - \lambda_1)}{\partial \mathbf{h}} = \sum_i \left(\frac{\partial D_{i,i}}{\partial \mathbf{h}} \right) - \frac{\partial \lambda_1}{\partial \mathbf{h}}$$

with \mathbf{h} being the lattice vector matrix

$$\mathbf{h} = \begin{bmatrix} h_1(1) & h_2(1) & h_3(1) \\ h_1(2) & h_2(2) & h_3(2) \\ h_1(3) & h_2(3) & h_3(3) \end{bmatrix}$$

with h_i being the lattice vectors. Like before we can use the the Hellman Feynman Theorem for the term $\frac{\partial \lambda_1}{\partial \mathbf{h}}$. This results in

$$\frac{\partial \lambda_1}{\partial \mathbf{h}} = \langle X_1 | \frac{\partial D}{\partial \mathbf{h}} | X_1 \rangle$$

The derivative of the matrix entries $D_{i,j}$ with respect to the lattice vectors is

$$\frac{\partial D_{i,j}}{\partial \mathbf{h}} = \sum_l^{l_{fp}} \frac{\partial V_i(l)}{\partial \mathbf{h}} V_j(l) + \frac{\partial V_j(l)}{\partial \mathbf{h}} V_i(l)$$

where we now need the derivative of the OM fingerprints V_i with respect to the lattice vectors.

To calculate the derivative of the OM fingerprints V_k with respect to the lattice vectors we can apply the chain rule so that we can use the already known derivation of the OM fingerprint with respect to the atomic positions $\frac{\partial V_k}{\partial R}$. It is important to note that the OM fingerprints V_k for atom k in the system is formed by putting Gaussian type orbitals only on all atoms within a given cutoff radius around the central atom k and then forming an overlap matrix from them. Therefore, we only need to consider the atomic positions \tilde{R}_j^k of all atoms j in the sphere around the central atom k . This leads to the fact that we now have two counting schemes, one for the atoms in the sphere and one for the atoms in the main cell. To deal with this we introduce a function $\text{index}(i, k)$ that maps atom number i from the sphere counting scheme of the central atom k to the main cell counting scheme that gives back the index of the corresponding atom in the main cell counting scheme. This results in

$$\frac{\partial V_k(l)}{\partial \mathbf{h}} = \sum_j^{N_{sp}} \frac{\partial V_k(l)}{\partial \tilde{R}_j^k} \frac{\partial \tilde{R}_j^k}{\partial \mathbf{h}}$$

with N_{sp} being the number of atoms in a sphere that is formed by the cutoff radius around the central atom k . Since the derivative of the overlap matrix fingerprint is invariant under the change of the counting scheme we get

$$\frac{\partial V_k}{\partial \tilde{R}_j^k} = \frac{\partial V_k}{\partial R_{\text{index}(j,k)}}$$

One needs to be aware of the fact that in periodic boundary conditions it is possible that multiple images of the same atom from the main cell can be inside the cutoff radius. The position of the atoms in the sphere around atom k can then be described as

$$\tilde{R}_i^k = R_{\text{index}(i,k)} + \mathbf{h} \cdot \mathbf{n}_{i,k} = \mathbf{h} \cdot R_{\text{index}(i,k)}^{\text{frac}} + \mathbf{h} \cdot \mathbf{n}_{i,k}$$

with

$$\mathbf{n}_{i,k} = \begin{bmatrix} a_{i,k} \\ b_{i,k} \\ c_{i,k} \end{bmatrix}$$

being the multiplier for atoms outside the periodic cell and

$$R_{\text{index}(i,k)}^{\text{frac}} = \begin{bmatrix} \alpha_{\text{index}(i,k)} \\ \beta_{\text{index}(i,k)} \\ \gamma_{\text{index}(i,k)} \end{bmatrix}$$

the atomic coordinates in fractional form of the atom belonging to index (i, k) in the main cell.

This results in

$$\frac{\partial \tilde{R}_i^k}{\partial h} = \begin{bmatrix} \alpha_{\text{index}(i,k)} + a_{i,k} & \beta_{\text{index}(i,k)} + b_{i,k} & \gamma_{\text{index}(i,k)} + c_{i,k} \\ \alpha_{\text{index}(i,k)} + a_{i,k} & \beta_{\text{index}(i,k)} + b_{i,k} & \gamma_{\text{index}(i,k)} + c_{i,k} \\ \alpha_{\text{index}(i,k)} + a_{i,k} & \beta_{\text{index}(i,k)} + b_{i,k} & \gamma_{\text{index}(i,k)} + c_{i,k} \end{bmatrix}$$

for atom i in the sphere counting scheme around the central atom k in the main cell counting scheme.
